指导教师：杨涛　　　　提交时间：2015 年 3 月 29 日

The task of Digital Image Processing

数字图像处理

School of Computer Science

No ：1

姓名：陈子问

学号：2012302396

班号：10011201

径向扭曲自校准的关键配置

摘要

在本文中,我们研究运动和结构的配置,导致径向扭曲估计中的固有的歧义(或三维重建与未知的径向扭曲)。通过分析径向扭曲图像的运动领域,我们解决临界表面对能导致相同的运动领域在不同径向扭曲和可能不同的相机运动。我们研究发现关键的属性配置,讨论了实际重要的配置,并且运用在真实的应用程序。我们将演示径向扭曲的影响的争议通过多视点重建与合成实验和实际实验。

1、介绍

运动结构（SFM）和自校准已经成为很习以为常的事情，就像最近的系统演示自动从大规模无标准的照片收藏集里 3 维重建【1,3,20】。这些系统表明他们对未知的径向扭曲的自校准的工作也很好。然而，它还没有被很好地理解当径向扭曲的自校准可能失败。这些工作最初的动机是被用于 SFM 地理调查，,在无人驾驶飞行器(无人机)是用来捕获的图像。这些拍摄系统有针对性的用语宽角度相机（例如：GoPro）为了覆盖到更大的区域，而且这些图像可能包含重大意义的径向扭曲。这些被捕获的图像经过 SFM 工具处理，例如，
Bundler【15】和 VisualSFM【21，19】，重建模型。然而这些无人机重建工作的同时，我们发现对于某些捕获的图像 SFM 软件产生错误的扭曲的 3d 模型和错误的径向扭曲（参见图 1)。这些径向扭曲估计的失败引发了我写了这篇文章。

三维重建，众所周知的是对某些配置的运动和结构是不完全确定的。这些所谓的关键配置已经被广泛的学习了，例如，对于欧式的重建与校准相机【5,12,9,7】和自校准线性相机【17,18,6,10】。在真实的应用中，相机通常有明显的径向扭曲需要准确的模型。但是，我们发现之前不久研究径向扭曲关键配置。这本文中，我们将要学习的配置是由于径向扭曲的歧义导致模棱两可的重建。我们的主要贡献有一下几点：
基于运动领域框架下解决模糊的配置一般径向扭曲模型;
我们解决了径向扭曲的关键表面和动作自校准使用新框架;
我们提出一个重要的关键配置,在实际的应用程序中经常出现的。
我们的研究结果可以指导图像捕获更好地避免不确定的径向扭曲估计，以及相应的显示当径向扭曲的预标准是需要的。其余部分组织如下：第二节讨论关键配置研究的背景。第三节介绍我们的框架分析径向扭曲自校准的歧义。我们调查关键配置及其属性在第 4,5 节，然后在第 6 节讨论一个很重要的配置存在于已知的运动方向。第 7 部分是结论和未来的工作。

2、背景

在过去的几十年中，研究人员调查了许多不同的三维重建问题的关键配置。给出任何相机运动，可能存在
大量的临界表面的三维重建是不确定的（不管规模）。裁定二次型或退化形式对于两个视图的重建和基于图像高速重建来说是个临界点[11，13，5，12]。对于三个或者更多的视图，可能存在临界椭圆四次欧式重建和摄影重建[9、4、8、7]。对于自校准的线性摄像机，存在一组关键动作下，三维重建是忽视结构而不确定的。Sturm 已经在一本著作中提出了关键动作的单方面的自校准【17】,并进一步研究这些不同的特性。然而，之前没有研究径向扭曲的关键配置的工作。在本文中，我们将研究这个新的关键配置问题。

几个特殊的简并组态的径向扭曲的自校准之前被报告过了。例如： Micuˇ sˇ´ık【14】和 Brito 【2】识别前进动作恢复退化情况下径向扭曲参数。此外 Micuˇ sˇ´ık 发现纯转化是模棱两可的，如果所有点位移与相机的转化在 XY 平面平行。这些实际上是特殊情况。本文将全面分析任意运动的关键配置。

尽管现代重建算法使用的离散点对应而不是运动领域，我们发现后者更方便分析径向扭曲。不同于复杂的非线性离散相机的径向扭曲之间的关系框架，径向扭曲可以方便的在一个连续的运动建模与衍生品，它可以解决很关键的配置没有任何的显式参数化。

在本文中，我们选择微分的方法；特别是在运动领域很有权威的人物——Horn。顺从的动作对应小的离散相机运动，对于重建视频序列，我们的研究结果是有价值的，相对争议可以积累大量的重建错误

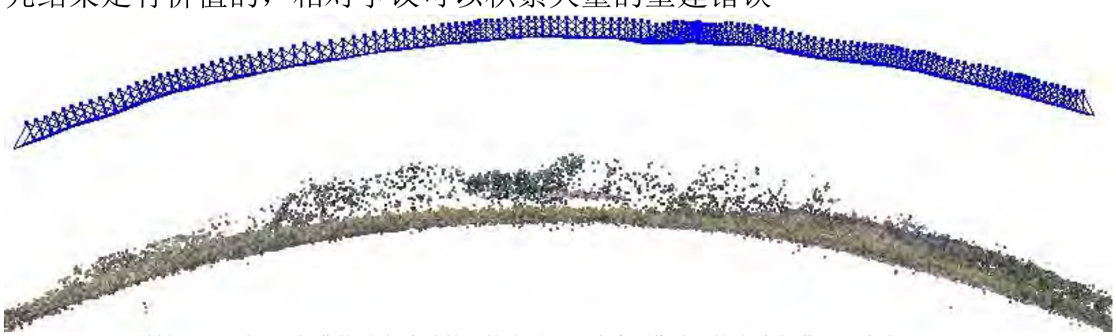

（a）关键配置导致明显扭曲的重建(大致持平的地面)。无失真图像验证的,径向扭曲不正确估计。如图 3 所示,我们使用合成数据集再生同样的问题。

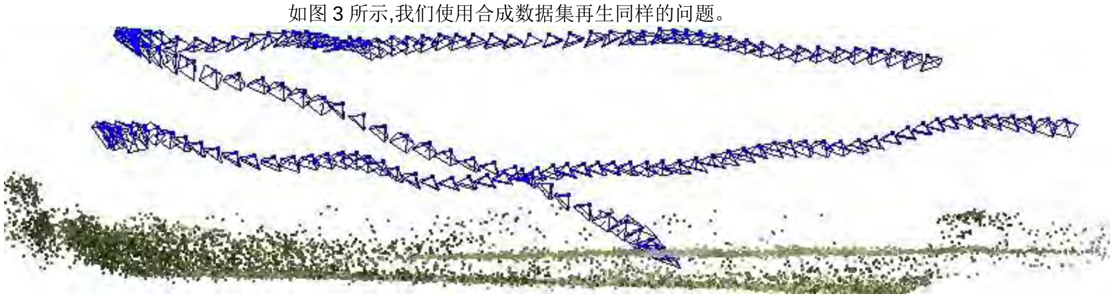

(b)重建一个典型的成功例子,径向扭曲估计。注意到的一个平坦的地面。

3、问题陈述

我们想要回答的问题是：给出两个不同径向扭曲的相机和可能的不同的运动，表面可能导致相同的运动领域是什么？这样的表面径向扭曲自校准的关键。因此大量的模糊运动领域由可能配置的相机对和相应的临界表面给予。

集中研究径向扭曲造成的歧义，我们假设这两个相机具有相同的线性特性。早些时候，一些模棱两可的线性特性已经得到充分的研究。如果分析包括多个不同的参数，如焦距，那么关于径向扭曲的研究将会更复杂，这些超出了本文的研究范围。

3.1、线性投射

首先，我们简要回顾一下用类似标记的方法的运动线性相机。不是一般性，我们要考虑相机图像的一致性。这个投射 p= $(x,y,1)^T$ 与其中一个三维点 $P = (X,Y,Z)^T$ 的关系是：$p = \frac{1}{P \cdot \hat{z}} P,$

其中 $z\hat{}= (0,0,1)^T$ 是观测方向。给出一个有关联的运动点 P^0

观测点的速率为：$p' = \frac{1}{P \cdot \hat{z}} \left(P' - (P' \cdot \hat{z})p\right)$

假设相机以一个瞬间直线移动的速率 t 和一个瞬间转动的速率 ω,这个三维点对应的相机速率是：

$$P^0 = -t + P \times \omega = -t + (P \cdot z\hat{})p \times \omega.$$

通过替换 P^0，我们得到图像速率：$p' = \frac{1}{Z} \left((t \cdot \hat{z})\, p - t\right) + [p, \omega, \hat{z}]\, p - p \times \omega,$

其中$[p,\omega,z\hat{}] = p\cdot(\omega \times z\hat{})$表示三维积。

3.2 一般径向扭曲

现在我们考虑到径向扭曲的图像。径向扭曲的典型假设中心和围绕主点，每张像圈主点对应着另一个新的不失真象圈，记住这个简单的机制，我们用一个基于以像圈规模的无参数径向扭曲模型。$f(r^2)$是像圈的比例因子 $r^2 = x^2 + y^2 = (p^Tp - 1)$

坐标映射从扭曲的图像不失真图像可以写成：undistort(p) = diag $\left(f(r^2),\ f(r^2),\ 1\right)\ p.$

我们将 $f(r^2)$作为径向扭曲的函数。为了方便，我们定义了两个有帮助的矩阵函数：

$F(r^2)$ = diag$(f, f, 1)$ and $F^0(r^2)$ = diag$(f',\ f',\ 0).$

通常，我们令 $f^0(r^2)$ 6= 0 因为 $f(r^2)$应该是一个常量。，从现在起，我们将省略参数(r^2)，f, f^0, F, 和 F^0 来简化方程，因此无形变的方程可以整合简化为 Fp。

这个无参数模型径向扭曲模型避免了可能的限制和显示参数化的复杂性。因此我们的研究结果并不局限与任何的特点径向扭曲参数化，并可以应用

于典型的近似线性相机和全方位中心相机。

值得指出的是 f(0)对应的焦距的倒数，如果我们参照焦距变化。虽然现实的径向扭曲 f(0)=1，本文将解决的 f(0)不确定值时的关键配置。我们分析集中于径向扭曲时，发现配置可能适用于额外的焦距变化。

3.3、径向扭曲下的投射

给定一个点 p 在一个扭曲的图像，我们可以用方程式 1 中 p 与 Fp 的关系获得不失真图像点的速率

Fp： $$(Fp)' = \frac{1}{Z}((t \cdot \hat{z})\, Fp - t) + [Fp, \omega, \hat{z}]\,(Fp) - (Fp) \times \omega.$$

此外，我们知道失真图像的速率 p^0 与不失真图像的速率$(Fp)^0$ 两者速度之间的关系：

$$(Fp)' = Fp' + F'(p^T p)' p = \left(F + 2F' p p^T\right) p'$$

上述的两种形式的$(Fp)^0$ 必须相等。

3.4、有争议的径向扭曲

假设一个无失真的相机运动轨迹$\{t_1,\ \omega_1\}$沿着深度 $Z_1(x,y)$产生了相同的运动轨迹动作$\{t_2,\ \omega_2\}$沿着深度 $Z_2(x,y)$在一个径向扭曲函数 f，下面是正确的公式:

$$\frac{(t_2 \cdot \hat{z})\, Fp - t_2}{Z_2} + [Fp, \omega_2, \hat{z}]\,(Fp) - (Fp) \times \omega_2 =$$
$$\left(F + 2F' p p^T\right) \left(\frac{(t_1 \cdot \hat{z})\, p - t_1}{Z_1} + [p, \omega_1, \hat{z}]\, p - p \times \omega_1 \right). \tag{2}$$

由于 z 分量图像的速度总是 0,平等给两个标量矢量约束,为解决 Z1(x,y)和 Z2(x,y)通常是足够的. 如此配置的{ t1,t2,ω1ω2,f,Z1,Z2 }被称为关键配置,Z1p 和 Z2Fp 的临界表面对{ω2,t1,t2,ω1 f }.在下一节中,我们将使用这个约束解决至关重要的表面,获得关键的动作。

一个不失真的相机不是去任何通用性的的关键表面。我们可以申请第二相机生产无失真的图像，尔第一个相机可以看着是失真的。同样，鉴于有两个不同相机的径向扭曲函数，我们可以应用一个不失真转换和不失真相机拍出的配置和另一个相机的相对失真。

4、关键配置

在本节中,我们解决至关重要的表面,然后得出任何表面的关键动作是至关重要的。

4.1、关键表面

我们暂时假设 t_2 6= 0，通过方程式 2 的点积 $t_2 \times Fp$ 我们可以消除 Z2,获得

解决第一临界表面 Z1 约束如下：

$$0=((Fp)\times\omega_2-F(p\times\omega_1))\cdot(t_2\times Fp)$$
$$+\frac{2}{Z_1}\left((t_1\cdot\hat{z})(p^Tp)-p^Tt_1\right)(F'p)\cdot(t_2\times Fp)$$
$$+\frac{1}{Z_1}[t_2,Ft_1,Fp]+2(p^Tp)\,[p,\omega_1,\hat{z}]\,(F'p)\cdot(t_2\times Fp)$$

$Fp=(f/f^0)(F^0p)$+zˆ，我们发现$(F^0p)\cdot(t_2\times Fp)=(F^0p)\cdot(t_2\times z\hat{})=f^0(t_2\times z\hat{})^Tp$。

通过扩展三维积，我们可以将上述的方程式写成：

$$0=((Fp)\times\omega_2-F(p\times\omega_1))\cdot(t_2\times Fp) \qquad (3)$$
$$+\frac{2f'}{Z_1}(t_1\cdot\hat{z})(p^Tp)(t_2\times\hat{z})^Tp-\frac{2f'}{Z_1}p^Tt_1(t_2\times\hat{z})^Tp$$
$$+\frac{1}{Z_1}(t_2\times Ft_1)^TFp+2f'\,(p^Tp)\,p^T(\omega_1\times\hat{z})(t_2\times\hat{z})^Tp,$$

定义了第一个关键表面 Z_1p

另一个方法观测关键表面的深度图：

$$Z_1=\frac{\begin{pmatrix}-2f'(t_1\cdot\hat{z})(p^Tp)(t_2\times\hat{z})^Tp+\\ 2f'p^T\,t_1(t_2\times\hat{z})^Tp-(t_2\times Ft_1)^TFp\end{pmatrix}}{\begin{pmatrix}((Fp)\times\omega_2-F(p\times\omega_1))\cdot(t_2\times Fp)\\ +2f'\,(p^Tp)\,p^T(\omega_1\times\hat{z})(t_2\times\hat{z})^Tp\end{pmatrix}}. \quad (4)$$

从除法来看显然当分母不为零的时候才有效。如果分子分母都是零，任何深度都满足方程 3，所以眼光应该放在临界表面上。如果只有分母为零，由此产生的深度将会无限，像点消失在关键表面。

通过方程的点积与 zˆ2×p,我们发现一双简单的临界表面之间的关系:

$$\frac{1}{Z_2}t_2\cdot(\hat{z}\times p)-\frac{1}{Z_1}(Ft_1)\cdot(\hat{z}\times p)\ =$$
$$-((Fp)\times\omega_2-F(p\times\omega_1))\cdot(\hat{z}\times p)$$

我们可以得到 Z_2 从 Z_1 当 $t_2\times z$ˆ 6= 0.第二个关键表面的深度图可以得到由：

$$Z_2=\frac{Z_1\ t_2\cdot(\hat{z}\times p)}{\left(Ft_1-\left((Fp)\times\omega_2-F(p\times\omega_1)\right)Z_1\right)\cdot(\hat{z}\times p)}. \qquad (6)$$

由 Z_2Fp.可以得出第二个关键表面，主要当 $t_2\times z$ˆ = 0，我们可以替代 p 来点积求出 Z_2,这里本文就不详述了。

图 2 演示了一些有趣的临界表面及其运动领域。临界表面产生径向扭曲且模糊的自校准运动。尽管有使用图像速率的差异，发现的退化情况[14]显然是唯一的一个特例。我们将讨论在第五节更关键的属性配置。

4.2、关键动作

有关键动作在任何表面都是模棱两可的恢复径向扭曲下存在，对于任何关键动作,方程 2 和 3 必须适用于任何深度 Z1 Z2,任何图像点 p,和任何径向扭曲,因此必须满足以下两个约束:

$$0 = \big((Fp) \times \omega_2 - F(p \times \omega_1)\big) \cdot (t_2 \times Fp) + 2f' \, (p^T p) \, p^T (\omega_1 \times \hat{z})(t_2 \times \hat{z})^T p, \tag{7}$$

$$0 = 2f'(t_1 \cdot \hat{z})(p^T p) \, (t_2 \times \hat{z})^T p - 2f' p^T t_1 (t_2 \times \hat{z})^T p + (t_2 \times F t_1)^T F p. \tag{8}$$

这两个方程可以被视为多项式函数的 p,f,和 f0,每学期的系数不同的顺序必须是零。

首先考虑一般情况下的 t_1 6= 0 和 t_2 6= 0,,方程 8 需要 $t_1 \times \hat{z} = t_2 \times \hat{z} = 0$,然后方程 7 需要 $\omega_1 \times \hat{z} = \omega_2 \times \hat{z} = 0$ 和 $\omega_1 = \omega_2$。即沿光轴平移和旋转光轴运动康复的径向变形至关重要。注意关键运动包括他们的结合。

当 t1 = 0 或 t2 = 0 时,我们发现没有真正关键的表面,除了关键在光轴旋转运动。如果 t1 = 0 和 t2 6 = 0,我们仍然能够获得方程 7 从方程 3,导致 $\omega_1 \times \hat{z} = \omega_2 \times \hat{z} = 0$ 和 $\omega_1 = \omega_2$。通过应用这些条件在方程 2 中,我们发现$(t_2 \cdot \hat{z}) Fp - t_2 = 0$,可满足所有 p 只有当 t2 = 0。同样我们必须 t1 = 0 时 t2 = 0。因此,径向扭曲不模棱两可的纯旋转除非绕光轴旋转。

总之，对于径向扭曲的自校准，我们发现下面面的关键动作：

$$t \times \hat{z} = \omega \times \hat{z} = 0. \tag{9}$$

歧义并不奇怪因为这些动作在光轴对称。前进运动退化[14，2]ω= 0 时是一个特例。另一方面,这些关键动作是关键动作的一个子集线性摄像机自校准[17]。在进一步分析关键的表面,我们将排除关键动作和任何纯旋转相机。

5、关键配置的性能

本节讨论一些关键的属性配置为径向扭曲自校准。

5.1、与不失真案例的比较

从方程 3 和 4 可以看出,径向扭曲的关键表面自校准度取决于高径向扭曲函数 f。相比之下,免于扭曲问题的关键表面可以通过设置 f = 1 和 f0 = 0,成为著名的简单判定二次型:

$$(P \times (\omega_2 - \omega_1)) \cdot (t_2 \times P) + (t_2 \times t_1)^T P = 0. \tag{10}$$

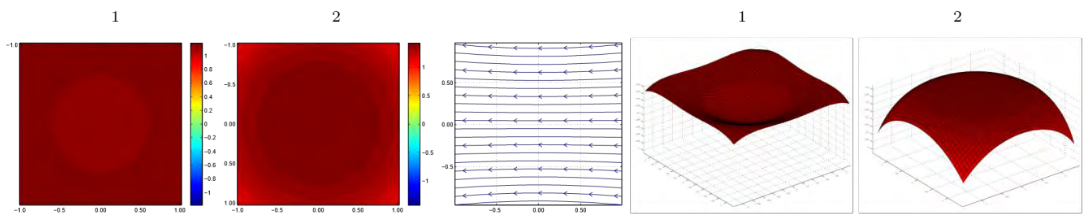

(a) $t_1 = t_2 = (1, 0, 0)^T$, $\omega_1 = (0, -0.1, 0)^T$, $\omega_2 = (0, -0.3, 0)^T$. The critical surfaces are rotationally symmetric. Note the convexity/concavity.

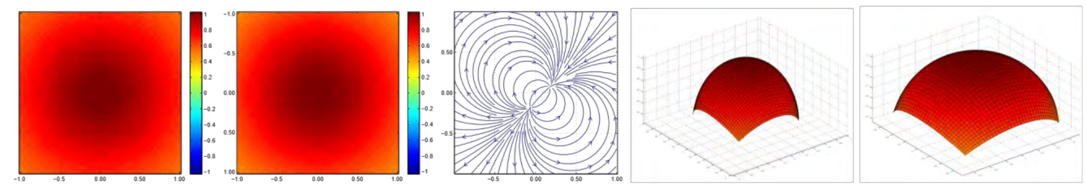

(b) $t_1 = t_2 = (-0.683853, -0.72962, 0.0)^T$, $\omega_1 = (0.695244, -0.6516340, -0.0766849)^T$, $\omega_2 = (0.692557, -0.649115, -0.0766849)^T$. The critical surfaces are rotationally symmetric. The motion field is similar to a magnetic field instead of being roughly parallel.

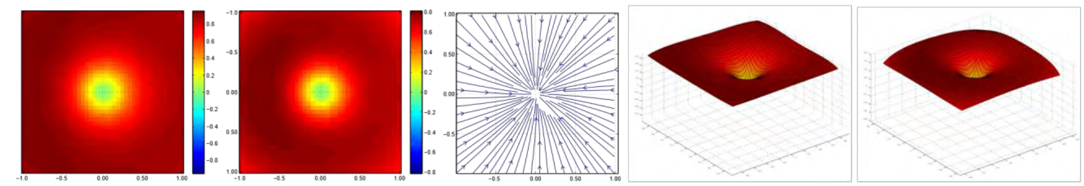

(c) $t_1 = t_2 = (-0.01, 0, -1)^T$, $\omega_1 = (0, 0.01, 0.05)^T$, $\omega_2 = (0, 0.099, 0.05)^T$. The translations are close to being forward in this example.

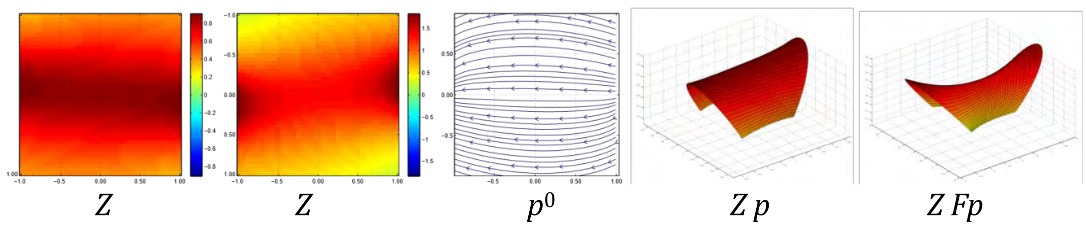

(d) $t1 = (0.850138, -0.526560, 0)^T$, $t_2 = (0.992789, -0.119871, 0)^T$, $\omega_1 = (0.600179, 0.419835, 0)^T$, $\omega_2 =$

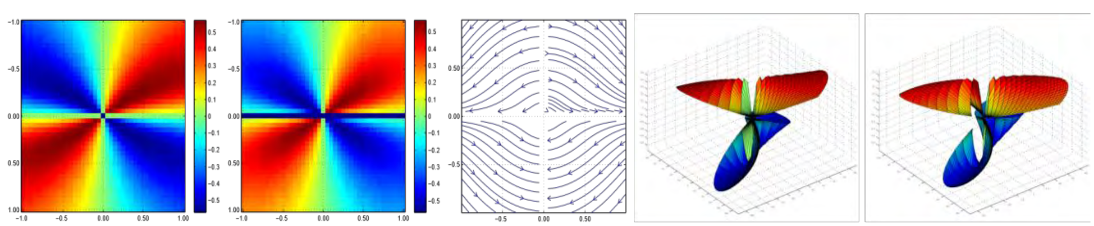

(e) $t_1 = t_2 = \omega_1 = \omega_2 = (1, 0, 0)^T$. Instead of being perpendicular, the translation and rotation are parallel in this example.

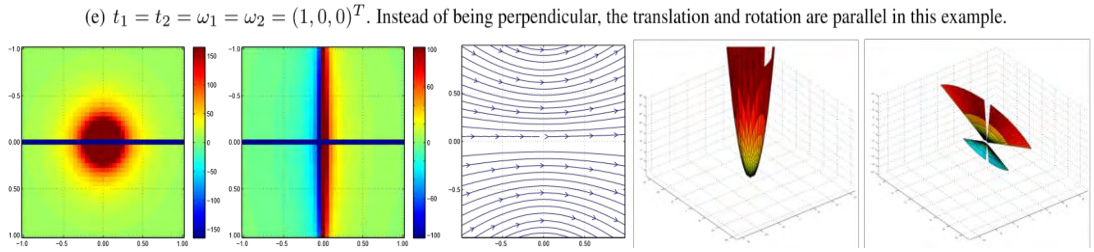

(0.080059,0.179102,0

(f) $t_1 = (1,0,0)^T$, $t2 = (0,0,1)^T$, $\omega_1 = \omega_2 = (0,1,0)^T$. 第二个镜头向前运动,第一次表面旋转对称的。

图 2：临界表面例子创建标识相机和径向扭曲函数: $f(r^2) = 1 + 0.1r^2 + 0.012r^4$ 从左到右 1）第一个深度图 2）第二个深度图 3）动作领域方向 4）第一个临界表面 5）第二个临界表面注意只有部分下方相对应的临界表面$(-1,1)\times(-1,1)$地区是可视化图像。

对于许多相机配置,径向扭曲的临界表面自校准实际上是类似于对应的二次型,并且可以被视为一种扭曲的版本的。一个示例配置如此关键的表面可以在图 2(d)。

当摄像机运动被认为是纯转化 $\omega_1 = \omega_2 = 0$ 或纯旋转 $t_1 = t_2 = 0$,临界表面不存在免于扭曲的情况。考虑径向扭曲时,存在前面讨论的关键动作但没有额外的临界表面。它已经表明,径向扭曲不模棱两可的纯旋转除了在光轴旋转。同样,发现径向扭曲不模棱两可的纯转化时除了沿光轴。

最大的区别将已知的情况下旋转 $\omega_1 = \omega_2$ 6= 0 和已知转化 $t_1 = t_2$ 6= 0 (忽略规模)。在这种情况下,众所周知,关键表面不存在免于扭曲问题[5]。与径向扭曲自检校相比,临界表面仍然存在,即使两个旋转和转化都知道 $t_1 - t_2 = \omega_1 - \omega_2 = 0$.。这可以从方程 4 因为 f^0 6= 0。如图 2 所示的例子如此关键的表面。

新型的临界表面特别有趣。这表明三维重建与未知的径向扭曲可能仍然是模棱两可的,即使转化和(或)旋转正确估计。

5.2、附加在光轴的旋转

对于任何运动和表面,满足方程 2 的配置,让我们考虑一个额外的光学轴,和旋转速度$\omega_1^\delta = \omega_1 + \delta\hat{z}$ 和
$\omega_2^\delta = \omega_2 + \delta\hat{z}$。方程 2 的左边之外$(Fp)\times(\delta\hat{z}) = f\delta(p\times\hat{z})$,和 F 等于除了右侧 $F(p \times (\delta\hat{z})) = f\delta(p \times \hat{z})$。因此,方程 2 仍然持有$\{t_1, \omega_1^\delta, t_2, \omega_2^\delta\}$相同的 Z1 和 Z2。即等于增加视轴的旋转速度不会改变临界表面,尽管运动领域的变化。

6、有趣的退化情况

如图所示的多项式方程 3 中不同程度方面,关键的表面一般是复杂的。我们可能感兴趣的是公约数的话,这样可以简化方程 4 中的深度。

6.1、常见的多项式因子

一个有趣的配置出现在我们的分析。
我们发现方程 3 第一临界表面有一个二阶多项式系数如下:

$$\Phi = p^T t_1 (t_2 \times \hat{z})^T p, \qquad (11)$$

当出现下述情况是：

$$t_1\cdot\hat{z} = t_2\cdot\hat{z} = 0,\ t_1 \times t_2 = 0, \text{ and } t_1\cdot t_2 \neq 0;$$
$$(\omega_1 - \omega_2)\cdot\hat{z} = 0 \text{ and } t_1\cdot\omega_1 = t_2\cdot\omega_2 = 0. \qquad (12)$$

摄像机运动可以看作之一的差模众所周知的情况如下:
•在一个球体而指向中心[16]。轨道与附加在光轴旋转运动。
•移动在飞机上,垂直于观察方向。这可以看作是在一个无限的范围($\omega \times \hat{z} = 0$)在上面的情况

可以看出 t_1, t_2, $(\omega_1\times\hat{z})$和 $(\omega_2\times\hat{z})$是平行的。注意关键表面将免于扭曲问题由于不存在已知的转化 t1× t2 = 0。

我们首先尝试简化涉及到 Fp 的向量积，也就是说$(Fp)\times\omega_2 - F(p\times\omega_1)$ 使用 5.2 节中讨论的不变性,我们可以假设 $\omega_1\cdot\hat{z} = \omega_2\cdot\hat{z} = 0$ 的$(\omega_1 - \omega_2)\cdot\hat{z} = 0$ 不改变关键的表面。通过使用事实 $p = (p - \hat{z}) + \hat{z}$,我们发现：

$$(Fp) \times \omega_2 - F(p \times \omega_1)$$
$$= f(p - \hat{z}) \times \omega_2 + \hat{z}\times \omega_2 - (p - \hat{z}) \times \omega_1 - f(\hat{z}\times \omega_1)$$
$$= (p - \hat{z}) \times (f\omega_2 - \omega_1) + \hat{z}\times (\omega_2 - f\omega_1), \qquad (13)$$

在该条件下,我们可以证明公式的分子和分母方程 4 被 Φ 整除。通过消除垂直的点积产生 0 和通过扩大四倍的乘积,我们可以改变如下:

$$
\begin{aligned}
&\big((Fp) \times \omega_2 - F(p \times \omega_1)\big) \cdot (t_2 \times Fp) \\
&= \begin{pmatrix} (p - \hat{z}) \times (f\omega_2 - \omega_1) \\ + \hat{z} \times (\omega_2 - f\omega_1) \end{pmatrix} \cdot \begin{pmatrix} f\, t_2 \times (p - \hat{z}) \\ + t_2 \times \hat{z} \end{pmatrix} \\
&= \Big((p - \hat{z}) \times (f\omega_2 - \omega_1)\Big) \cdot \Big(f\, t_2 \times (p - \hat{z})\Big) \\
&= \big((p - \hat{z}) \cdot t_2\big) \; \big((p - \hat{z}) \cdot (f^2\omega_2 - f\omega_1)\big) \\
&= -p^T \big((f^2\omega_2 - f\omega_1) \times \hat{z}\big) \big(t_2 \times \hat{z}\big)^T p,
\end{aligned}
$$

可以除以 Φ 因为 t_1 k $(\omega_1 \times z\hat{})$ k $(\omega_2 \times z\hat{})$，同样，分母中公式 $2f^0\,(p^Tp)p^T(\omega_1 \times z\hat{})(t_2 \times z\hat{})^Tp$ 可以除以 Φ 因为 t_1 k $(\omega_1 \times z\hat{})$，至于分子的式子 $(t_1 \cdot z\hat{})(p^Tp)(t_2 \times z\hat{})^Tp$ and $(t_2 \times Ft_1)^T Fp$ 变为 0，只剩下式子 $2f^0\, p\, t_1(t_2 \times z\hat{})\, p = 2f^0\,\Phi$.

公约数 Φ 本身定义了两个关键的位面 $t_1^T p = 0$ 和 $(t_2 \times z\hat{})^Tp = 0$。两个位面不太受人关注，因为相机中心是在位面和他们也垂直于图像平面。我们主要谈论简化的深度，抛开这里的位面。

6.2、旋转对称表面

通过用公约数 Φ，第一个临街面可以简化为：

$$
\begin{aligned}
Z_1 &= \frac{2f'\, p^T t_1 (t_2 \times \hat{z})^T\, p}{\begin{pmatrix} -p^T \big((f^2\omega_2 - f\omega_1) \times \hat{z}\big) \big(t_2 \times \hat{z}\big)^T p \\ + 2\, f'\, (p^T p)\, p^T (\omega_1 \times \hat{z})\, (t_2 \times \hat{z})^T\, p \end{pmatrix}} \\
&= \frac{2\,(t_1 \cdot t_2) f'}{\begin{pmatrix} -(t_2 \cdot (\omega_2 \times \hat{z})) f^2 + (t_2 \cdot (\omega_1 \times \hat{z})) f \\ + 2\,(t_2 \cdot (\omega_1 \times \hat{z}))(p^T p) f' \end{pmatrix}}, \quad (14)
\end{aligned}
$$

使一个深度值为每个图像圈 $r^2 = x^2 + y^2 = p^Tp - 1.$。生成的临界表面在光轴旋转对称。

第二个临界表面可以解决相应的使用两个深度图之间的关系。方程 13 允许简化如下:

$$((Fp) \times \omega_2 - F(p \times \omega_1)) \cdot (z\hat{} \times p) = (z\hat{} \times (\omega_2 - f\,\omega_1)) \cdot (z\hat{} \times p).$$

第二个临界面可以简化如下：

$$
\begin{aligned}
Z_2 &= \frac{Z_1\; t_2 \cdot (\hat{z} \times p)}{(Ft_1 - Z_1\,(\hat{z} \times (\omega_2 - f\,\omega_1))) \cdot (\hat{z} \times p)} \\
&= \frac{(t_1 \cdot t_2)\; Z_1}{(t_1 \cdot t_1)\, f - t_1 \cdot\, (\hat{z} \times (\omega_2 - f\,\omega_1))\, Z_1}, \qquad (15)
\end{aligned}
$$

这是再一次旋转对称。[1]给出了两个例子这样的临界表面在图 2(a)和 2(b)。两个临界表面都是旋转对称的,但有不同的弯曲度,甚至不同曲率的迹象。

对于一个视角有限的相机，部分临街面可以是近似球形的，也可以是近似平面形的，甚至根据运动和径向扭曲函数断定是一个完美的平面。例如：

$f(r^2) = 1/(1-\lambda r^2)$和 $\omega_1 \times \hat{z} = 0$，我们给出一个向量深度$Z_1 = \frac{4\lambda\,(t_1 \cdot t_2)}{t_2 \cdot (\hat{z} \times \omega_2)}$

让我们重温无人机捕捉如图 1 所示(a),相机的移动与地面平行,相机指向地面。可见的表面相对于每个相机近似平面的在径向扭曲,从而造成歧义估计。

6.3、实验

我们设计两个综合图像序列来验证径向扭曲歧义和展示其对多视点三维重建的影响。我们提供无噪声的功能协调和完美匹配 VisualSFM[19],并自动比较重建模型真实的模型。虽然不是基于速率的重建方法,我们希望相同的歧义与密集采样图像序列。

首先,如图 3 所示,我们上面移动相机平面点网格以恒定的高度,保持相机指向飞机。扭曲的图像生成的径向扭曲 $f(r^2) = 1 + \lambda r^2$, $\lambda = 0.2$。这可以被视为一个理想的版本的捕获在图 1(a)。类似于真正的捕捉,合成数据集的自动重建产生错误的扭曲的 3 d 模型由于径向扭曲的歧义。其次,我们使用一个网格点上一个完美的球体。相机移动一起居中外球体,球体中心。扭曲的图像生成的径向扭曲 $f(r^2) = 1+\lambda r^2$, $\lambda = -0.2$。球面是旋转对称和模棱两可的重建。如图 4 所示,自动重建产生一个凹面。

实验表明,多视点重建可以导致失败自校准径向扭曲在某些关键配置。重建的失真是当地的曲率差异引起的临界表面双曲率误差积累和全球的持久模棱两可的整个捕获。

典型的 SfM 系统初始化新相机的径向扭曲为零和依赖包调整优化参数。我们观察倾向于低估径向扭曲近似堕落化配置,这可以部分解释为零初始化。径向扭曲的歧义是可能导致重大错误时径向扭曲是切断或初始估计太不准确的。还要注意会有更多歧义时使用更多的径向扭曲参数,例如, $f(r^2) = 1 + \lambda_1 r^2 + \lambda_2 r^4$ 相比 $f(r^2) = 1 + \lambda_1 r^2$.

7. 结论与未来展望

介绍了径向扭曲的关键配置自校准一般径向扭曲模型。结果表明,径向扭曲引入了一种新的模糊 SfM。不同于纯粹的线性摄像机参数化,关键表面存在甚至知道翻译和已知旋转径向扭曲。特别是,本文展示了几乎重要关键配置,应避免在实际捕获径向扭曲自校准。本文不是一个完整的研究所有可能的歧义与径向扭曲。作者希望进行数值稳定性研究近似退化配置和扩展调查在未来从连续动作到离散的观点。

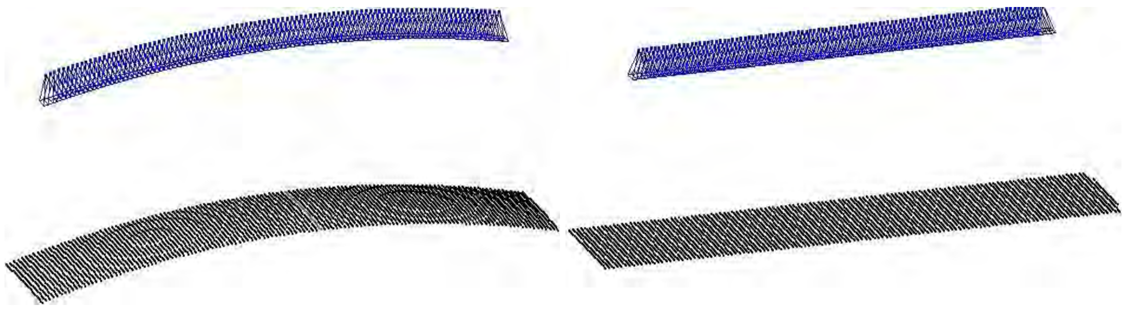

(a) The automatic reconstruction estimates an incorrect $\lambda^0 = 0.02$ (b) The ground-truth reconstruction using the known $\lambda = 0.2$

图 3：重建的平面网格点。蓝色的锥形是黑点的相机和重建的点。

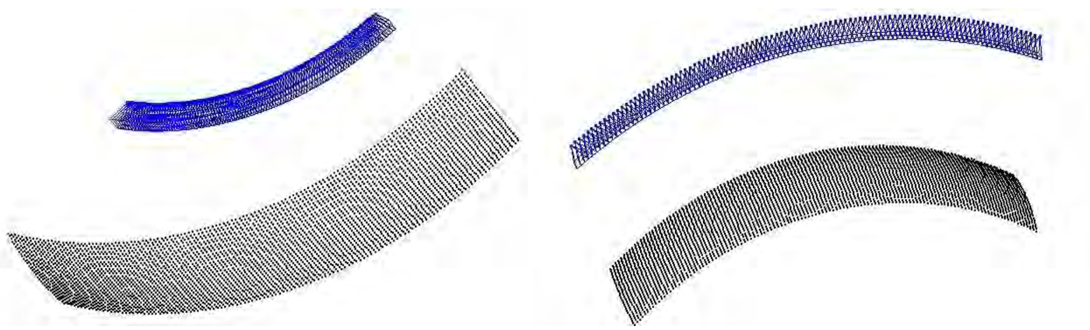

(a) The automatic reconstruction estimates an incorrect $\lambda^0 = 0.025$(b) The ground-truth reconstruction using the known $\lambda = -0.2$

图 4：重建网格点的一个球体。蓝色的锥形是黑点的相机和重建的点。

确认作者衷心感谢托马斯 Groninger 提供两个无人机数据集

8、参考文献

[1] S. Agarwal, N. Snavely, I. Simon, S. M. Seitz, and R. Szeliski. Building Rome in a day. In *ICCV*, 2009.

[2] J. H. Brito, R. Angst, K. Koser, and M. Pollefeys. Radial¨ distortion self-calibration. In *CVPR*, 2013.

[3] D. Crandall, A. Owens, N. Snavely, and D. P. Huttenlocher. Discrete-continuous optimization for large-scale structure from motion. In *CVPR*, 2011.

[4] R. I. Hartley. Ambiguous configurations for 3-view projective reconstruction. In *ECCV*, pages 922–935, 2000.

[5] B. K. P. Horn. Motion fields are hardly ever ambiguous. *IJCV*, 1(3):259–274, 1987.

[6] F. Kahl. Critical motions and ambiguous euclidean reconstructions in auto-calibration. In *ICCV*, volume 1, pages 469–475, 1999.

[7] F. Kahl and R. Hartley. Critical curves and surfaces for euclidean reconstruction. In *ECCV*, pages 447–462, 2002.

[8] F. Kahl, R. Hartley, and K. Astrom. Critical configurations for n-view projective reconstruction. In *CVPR*, pages 158–163, 2001.

[9] F. Kahl and B. Triggs. Critical motions in euclidean structure from motion. In *CVPR*, volume 2, 1999.

[10] F. Kahl, B. Triggs, and K. Astr˚ om.¨ Critical motions for auto-calibration when some intrinsic parameters can vary. *JMIV*, 13(2):131–146, 2000.

[11] H. C. Longuet-Higgins. Visual ambiguity of a moving plane. *Proceedings of The Royal Society of London, Biological Sciences*, pages 165–175, 1984.

[12] S. Maybank. Theory of reconstruction from image motion. 1993.

[13] S. J. Maybank. The angular velocity associated with the optical flow field due to a single moving rigid plane. In *ECAI*, pages 641–644, 1984.

[14] B. Micuˇ sˇ´ık and T. Pajdla. Structure from motion with wide circular field of view cameras. *TPAMI*, 28(7):1135–1149, 2006.

[15] N. Snavely, S. Seitz, and R. Szeliski. Photo tourism: exploring photo collections in 3D. In *SIGGRAPH*, pages 835–846, 2006.

[16] P. Sturm. A case against kruppa's equations for camera self-calibration. *TPAMI*, 22(10):1199–1204, 2000.

[17] P. F. Sturm. Critical motion sequences for monocular self-calibration and uncalibrated euclidean reconstruction. In *CVPR*, pages 1100–1105, 1997.

[18] P. F. Sturm. Critical motion sequences for the self-calibration of cameras and stereo systems with variable focal length. In *BMVC*, 1999.

[19] C. Wu. VisualSFM: A visual structure from motion system, 2011. http://ccwu.me/vsfm.

[20] C. Wu. Towards linear-time incremental structure from motion. In *3DV*, 2013.

[21] C. Wu, S. Agarwal, B. Curless, and S. M. Seitz. Multicore bundle adjustment. In *CVPR*, 2011.

以下为原文：

Critical Configurations For Radial Distortion Self-Calibration

Changchang Wu

Google Inc.

Abstract

In this paper, we study the configurations of motion and structure that lead to inherent ambiguities in radial distortion estimation (or 3D reconstruction with unknown radial distortions). By analyzing the motion field of radially distorted images, we solve for critical surface pairs that can lead to the same motion field under different radial distortions and possibly different camera motions. We study the properties of the discovered critical configurations and discuss the practically important configurations that often occur in real applications. We demonstrate the impact of the radial distortion ambiguity on multi-view reconstruction with synthetic experiments and real experiments.

1. Introduction

Structure from motion (SfM) and self-calibration have become commonplace, as recent systems demonstrate automatic 3D reconstructions from large-scale uncalibrated photo collections [1, 3, 20]. These systems show that the self-calibration of unknown radial distortions normally works well. However, it has not been well understood when the self-calibration of radial distortion could fail.

This work was initially motivated by the application of SfM in geographic survey, where Unmanned Aerial Vehicles (UAVs) are used to capture the images. These capture systems typically use wide-angle cameras (e.g. GoPro) in order to cover large areas, and the images may contain significant radial distortions. The captured images are then processed by SfM tools, for example, Bundler [15] and VisualSFM [21, 19], to reconstruct the ground models. While these UAV reconstructions usually work, we find for certain captures that the SfM softwares produce incorrectly distorted 3D models along with incorrect estimations of radial distortions (See Figure 1). These failures in radial distortion estimation inspired this paper.

3D reconstruction is well known to have ambiguities for certain configurations of motion and structure. These so called critical configurations have been extensively studied, for example, for Euclidean reconstruction with calibrated cameras [5, 12, 9, 7] and self-calibration of linear cameras [17, 18, 6, 10]. In real applications, cameras often have significant radial distortions that need to be explicitly modeled. However, we find little previous study on the critical configurations for radial distortion. In this paper, we will study the configurations that can lead to ambiguous reconstructions due to the ambiguity of radial distortion. Our main contributions are the following:

- A motion field based framework for solving ambiguous configurations under a general radial distortion model;
- We solve for the critical surfaces and motions for radial distortion self-calibration using the new framework;
- We present an important critical configuration that often occurs in practical applications.

Our findings can guide image capture to better avoid ambiguous radial distortion estimation, and correspondingly show when pre-calibration of radial distortion is necessary.

The remainder is organized as follows: Section 2 discusses the background of the critical configuration study. Section 3 introduces our framework for analyzing the ambiguities for radial distortion self-calibration. We investigate the critical configurations and their properties in Section 4 and 5, and then discuss in Section 6 a practically important configuration that exists under known motion directions. Conclusions and future work are given in Section 7.

2. Background

In the past several decades, researchers have investigated the critical configurations for many different 3D reconstruction problems. Given any camera motion, there may exist a family of possible critical surfaces for which 3D reconstruction is ambiguous (regardless of the scale). Ruled quadrics or their degenerate forms are critical surfaces for two view reconstruction and image velocity based reconstruction [11, 13, 5, 12]. For three views or more, critical elliptic quartics may exist for Euclidean reconstruction and projective reconstruction [9, 4, 8, 7]. For the self-calibration of linear cameras, there exist a set of critical motions under which 3D reconstruction is ambiguous regardless of the structures. A complete study of such critical motions for monocular self-calibration has been presented by Sturm [17], and further study for varying intrinsics can be found in [18, 10]. However, no prior work has examined the critical configurations for radial distortion. In this paper, we will study this new critical configuration problem.

A few special degenerate configurations for radial distortion self-calibration have been reported previously. For example, Micuˇ sˇ´ık *et al*. [14] and Brito *et al*. [2] recognize forward motion as a degenerate case for recovering radial distortion parameters. Additionally, Micuˇ sˇ´ık *et al*. [14] find pure translation to be ambiguous if all point displacements are parallel to the camera's translation in XY plane. These are in fact special cases. This paper will present a full analysis of the critical configurations for arbitrary motions.

Although modern reconstruction algorithms use discrete point correspondences instead of motion fields, we find the latter more convenient for analyzing radial distortions. Unlike the complicated non-linear relationship between the radial distortions in discrete camera frames, the radial distortion in a continuous motion can be conveniently modeled with derivatives, which allows to solve for the critical configurations without any explicit parametrization. In this paper, we opt for the differential approach, in particular, on top of the motion field study by Horn [5]. As deferential motions correspond to small discrete camera motions, our findings are valuable for the reconstruction of video sequences, where the relative ambiguities can accumulate to large reconstruction errors.

(a) A critical configuration that leads to a significantly distorted reconstruction (of the roughly flat ground). As verified by the undistortedimages, the radial distortion is not correctly estimated. See Figure 3 where we re-produce the same problem using a synthetic dataset.

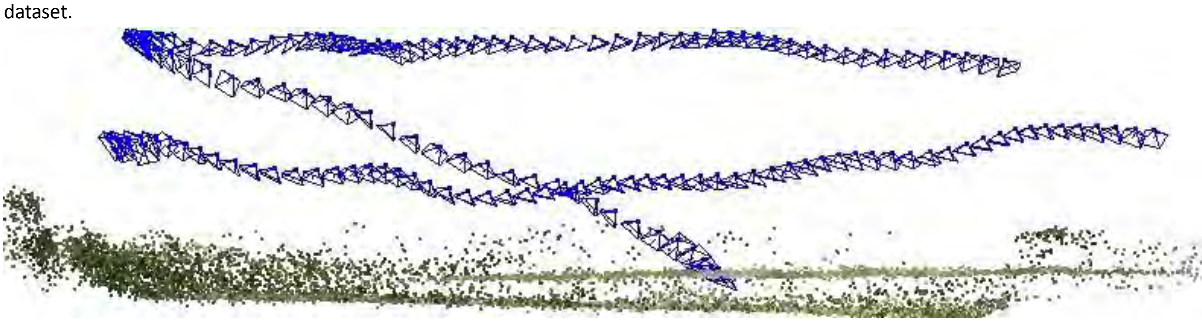

(b) A typical successful reconstruction example, where radial distortions are well estimated. Notice one of the flat ground surface.

Figure 1. Reconstruction of two GoPro UAV sequences using VisualSFM [19] (similar results are produced by Bundler [15]). No radial distortion calibration is specified to the software. As shown by the blue pyramids, the camera points straight downward and moves parallel to the ground in the first capture. In the second capture, the camera has more variations in moving directions and viewing directions.

3. Problem formulation

The question we want to answer is the following: *given two cameras with different radial distortions and* *possibly different motions, what surfaces could lead to the same motion field?* Such surfaces would be critical for radial distortion self-calibration. Accordingly, the family of ambiguous motion fields is given by the possible configurations of camera pairs and their corresponding critical surfaces.

To focus on the ambiguity caused by radial distortions alone, we assume the two cameras to have the same linear intrinsics. As reviewed earlier, the ambiguity of the linear intrinsics has already been well studied. If the analysis includes more varying parameters, such as focal length, the ambiguity would be a larger super-set of the radial distortion related ambiguity, the study of which is beyond the scope of this paper.

3.1. Linear projection

First, we briefly review the motion field of linear cameras using notations similar to [5]. Without loss of generality, we consider the image of an identity camera. The projection $p = (x,y,1)^T$ of a 3D point $P = (X,Y,Z)^T$ is

$$p = \frac{1}{P \cdot \hat{z}} P,$$

where $\hat{z} = (0,0,1)^T$ is the viewing direction. Given a relative moving speed P^0, the velocity of its observation is

$$p' = \frac{1}{P \cdot \hat{z}} \left(P' - (P' \cdot \hat{z})p\right).$$

Suppose the camera moves with an instantaneous translational velocity t and an instantaneous rotational velocity ω, the velocity of the 3D point relative to the camera is

$$P^0 = -t + P \times \omega = -t + (P \cdot \hat{z})p \times \omega.$$

By substituting P^0, we obtain the image velocity

$$p' = \frac{1}{Z}\left((t \cdot \hat{z})\, p - t\right) + [p, \omega, \hat{z}]\, p - p \times \omega, \tag{1}$$

where $[p,\omega,\hat{z}] = p \cdot (\omega \times \hat{z})$ denotes the triple product.

3.2. General radial distortion

Now we consider the images with radial distortion. With a typical assumption of the radial distortion being central and centered around the principal point, each image circle around the principal point corresponds to another rescaled image circle in the undistorted image. With this simple mechanism in mind, we use a parameter-free radial distortion model based on the scaling of the image circles. Let $f(r^2)$ be the scaling factor for the image circle $r^2 = x^2 + y^2 = (p^Tp - 1)$, the coordinate mapping from the distorted image to the undistorted image can be written as: undistort(p) = diag $\left(f(r^2),\ f(r^2),\ 1\right) p.$

We will refer to $f(r^2)$ as the *radial distortion function*. For convenience, we define two helper matrix functions

$F(r^2)$ = diag$(f, f, 1)$ and $F^0(r^2)$ = diag$(f',\ f',\ 0)$.

In general, we have $f^0(r^2)$ 6= 0 because $f(r^2)$ should not be a constant. From now on, we will omit the argument (r^2) for f, f^0, F, and F^0 to simplify the equations, so the undistorted coordinate can be simply written as Fp.

This parameter-free radial distortion model avoids the possible limitations and complexities of explicit parametrization. As a result, our findings will not be limited to any specific radial distortion parametrization, and can be applied to both typical near-linear cameras and central omni-directional cameras.

It is worth pointing out that $f(0)$ would correspond to the reciprocal of focal length if we also model the variation of focal length. Although real radial distortions have $f(0) = 1$, this paper will solve the critical configurations without explicit assumptions on $f(0)$. While our analysis focuses on just radial distortion, the discovered configurations may be applied to additional variations of focal length.

3.3. Projection under radial distortion

Given a point p in a distorted image, we can obtain the velocity of the undistorted image point Fp by substituting p with Fp into Equation 1:

$$(Fp)' = \frac{1}{Z}((t \cdot \hat{z})\, Fp - t) + [Fp, \omega, \hat{z}]\,(Fp) - (Fp) \times \omega.$$

In addition, we know the relationship between the velocity p^0 in the distorted image and the velocity $(Fp)^0$ in the undistorted image from differentiation:

$$(Fp)' = Fp' + F'(p^Tp)'p = \left(F + 2F'pp^T\right) p'.$$

The above two forms of $(Fp)^0$ must be equal to each other.

3.4. Ambiguous radial distortion

Suppose a distortion-free camera with motion $\{t_1,\ \omega_1\}$ along with depth $Z_1(x,y)$ produces the same motion field as does a motion $\{t_2,\ \omega_2\}$ along with depth $Z_2(x,y)$ under a radial distortion function f, the following holds true:

$$\frac{(t_2 \cdot \hat{z})\, Fp - t_2}{Z_2} + [Fp, \omega_2, \hat{z}]\,(Fp) - (Fp) \times \omega_2 =$$
$$\left(F + 2F'pp^T\right)\left(\frac{(t_1 \cdot \hat{z})\, p - t_1}{Z_1} + [p, \omega_1, \hat{z}]\, p - p \times \omega_1\right). \tag{2}$$

Since the Z-component of the image velocity is always 0, the vector equality gives two scalar constraints, which are usually sufficient for solving $Z_1(x,y)$ and $Z_2(x,y)$. Such a configuration of $\{t_1,t_2,\omega_1,\omega_2,f,Z_1,Z_2\}$ is called a critical configuration, where Z_1p and Z_2Fp are the critical surface pair for $\{t_1,t_2,\omega_1,\omega_2,f\}$. In the next Section, we will use this constraint to solve for the critical surfaces and derive critical motions.

The configuration with one distortion-free camera does not lose any generality in terms of critical surfaces. We can apply the undistortion transformation of the second camera to produce the undistorted image, for which the first camera can be seen as the distorted one. Similarly, given two cameras that have different radial distortion functions, we can apply one of the undistortion transformations and produce the configuration of one distortion-free camera and another camera with a relative distortion.

4. Critical configurations

In this section, we solve for the critical surfaces and then derive the critical motions where any surface is critical.

4.1. Critical surfaces

For a moment we will assume t_2 6= 0. By taking the dot-product of the Equation 2 with $t_2 \times Fp$, we can eliminate Z_2 and obtain the constraint for solving the first critical surface Z_1 as follows

$$\begin{aligned} 0 &= ((Fp)\times\omega_2 - F(p\times\omega_1))\cdot(t_2\times Fp) \\ &+ \frac{2}{Z_1}\left((t_1\cdot\hat{z})(p^Tp) - p^Tt_1\right)(F'p)\cdot(t_2\times Fp) \\ &+ \frac{1}{Z_1}[t_2, Ft_1, Fp] + 2(p^Tp)\,[p,\omega_1,\hat{z}]\,(F'p)\cdot(t_2\times Fp) \end{aligned}.$$

Given $Fp = (f/f^0)(F^0p)+\hat{z}$, we find $(F^0p)\cdot(t_2\times Fp) = (F^0p)\cdot(t_2\times\hat{z}) = f^0(t_2\times\hat{z})^Tp$. By further expanding the triple products, we can rewrite the above equation as

$$\begin{aligned} 0 &= ((Fp)\times\omega_2 - F(p\times\omega_1))\cdot(t_2\times Fp) \\ &+ \frac{2f'}{Z_1}(t_1\cdot\hat{z})(p^Tp)(t_2\times\hat{z})^Tp - \frac{2f'}{Z_1}p^Tt_1(t_2\times\hat{z})^Tp \\ &+ \frac{1}{Z_1}(t_2\times Ft_1)^TFp + 2f'\,(p^Tp)\,p^T(\omega_1\times\hat{z})(t_2\times\hat{z})^Tp, \end{aligned} \tag{3}$$

which defines the first critical surface Z_1p. Another way to view this critical surface is a depthmap:

$$Z_1 = \frac{\begin{pmatrix} -2f'(t_1\cdot\hat{z})(p^Tp)(t_2\times\hat{z})^Tp + \\ 2f'p^T\,t_1(t_2\times\hat{z})^Tp - (t_2\times Ft_1)^TFp \end{pmatrix}}{\begin{pmatrix} ((Fp)\times\omega_2 - F(p\times\omega_1))\cdot(t_2\times Fp) \\ +2f'\,(p^Tp)\,p^T(\omega_1\times\hat{z})(t_2\times\hat{z})^Tp \end{pmatrix}}. \tag{4}$$

The depth from such a division is obviously valid only when the denominator is non-zero. If both the numerator and the denominator are zero, any depth satisfies Equation 3, so the viewing ray would lie on the critical surface. In case only the denominator is zero, the resulting depth would be infinite, where the image point is a vanishing point of the critical surface.

By taking the dot-product of Equation 2 with $\hat{z}\times p$, we find a simple relationship between the critical surface pair:

$$\begin{aligned} \frac{1}{Z_2}t_2\cdot(\hat{z}\times p) - \frac{1}{Z_1}(Ft_1)\cdot(\hat{z}\times p) &= \\ -\,((Fp)\times\omega_2 - F(p\times\omega_1))\cdot(\hat{z}\times p)& \end{aligned},$$

which allows us to obtain Z_2 from Z_1 when $t_2\times\hat{z}$ 6= 0. The depthmap of the second critical surface can be obtained as:

$$Z_2 = \frac{Z_1\;t_2\cdot(\hat{z}\times p)}{\left(Ft_1 - \left((Fp)\times\omega_2 - F(p\times\omega_1)\right)Z_1\right)\cdot(\hat{z}\times p)}. \tag{6}$$

The second critical surface is then given by $Z_2\,F\,p$. Note when $t_2\times\hat{z} = 0$, we can still solve for Z_2 by taking dot-product with p instead, which this paper will skip.

Figure 2 demonstrates some interesting critical surfaces and their motion fields. The critical surfaces yield the motion fields that are ambiguous for radial distortion selfcalibration. Despite the difference of using image velocity here, the degenerate case found by [14] is apparently only a special case. We will discuss more properties of the critical configurations in Section 5.

4.2. Critical motions

There exist critical motions under which any surface is ambiguous for recovering radial distortions. For any critical motion, Equation 2 and 3 must hold true for any depth Z_1 and Z_2, any image point p, and any radial distortion, therefore the following two constraints must be satisfied:

$$0 = \left((Fp)\times\omega_2 - F(p\times\omega_1)\right)\cdot(t_2\times Fp) + 2f'\,(p^Tp)\,p^T(\omega_1\times\hat{z})(t_2\times\hat{z})^Tp, \tag{7}$$

$$0 = 2f'(t_1\cdot\hat{z})(p^Tp)\,(t_2\times\hat{z})^Tp - 2f'p^T\,t_1(t_2\times\hat{z})^Tp + (t_2\times Ft_1)^TFp. \tag{8}$$

The two equations can be viewed as polynomial functions of p, f, and f^0, where the coefficient for each term of different order must be zero.

Consider firstly the general case of t_1 6= 0 and t_2 6= 0, Equation 8 requires $t_1\times\hat{z} = t_2\times\hat{z} = 0$, and Equation 7 then requires $\omega_1\times\hat{z} = \omega_2\times\hat{z} = 0$ and $\omega_1 = \omega_2$. That is, translation along the optical axis and rotation around the

optical axis are critical motions for recovering radial$\omega_1 = \omega_2$. By applying these conditions in Equation 2, we find $(t_2 \cdot \hat{z})Fp - t_2 = 0$, which can be satisfied for all p only when $t_2 = 0$. Similarly we must have $t_1 = 0$ when $t_2 = 0$. Therefore, radial distortion is not ambiguous for pure rotations unless the rotation is around the optical axis.
In summary, for the self-calibration of radial distortion, we find the following critical motions:

$$t \times \hat{z} = \omega \times \hat{z} = 0. \tag{9}$$

The ambiguity is not surprising since such motions are symmetric around the optical axis. The forward motion degeneracy reported in [14, 2] is a special case when $\omega = 0$. On the other hand, these critical motions is a subset of the critical motions for the linear camera self-calibration [17]. In further analysis of critical surfaces, we will exclude the critical motions and any pure rotation cameras.

1. Properties of the critical configurations

This section discusses a few properties of the critical configurations for radial distortion self-calibration.

1.1. Comparison with the distortion-free case

It can be seen from Equation 3 and 4 that the critical surfaces for radial distortion self-calibration have high degrees depending on the radial distortion function f. In comparison, the critical surfaces for the distortion-free

1 2 1 2

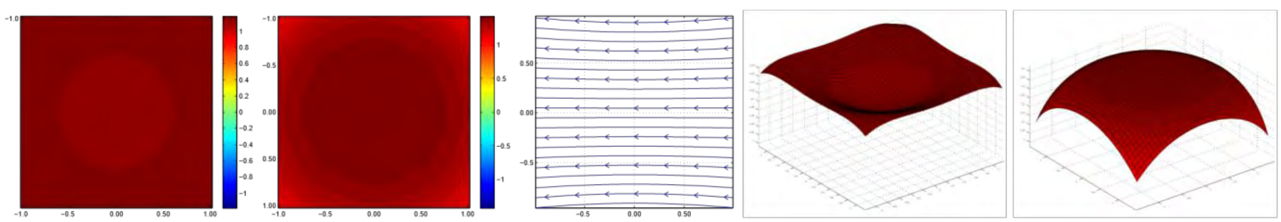

(a) $t_1 = t_2 = (1, 0, 0)^T$, $\omega_1 = (0, -0.1, 0)^T$, $\omega_2 = (0, -0.3, 0)^T$. The critical surfaces are rotationally symmetric. Note the convexity/concavity.

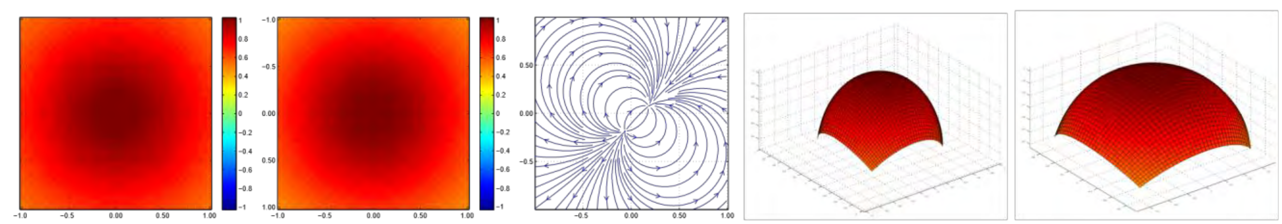

(b) $t_1 = t_2 = (-0.683853, -0.72962, 0.0)^T$, $\omega_1 = (0.695244, -0.6516340, -0.0766849)^T$, $\omega_2 = (0.692557, -0.649115, -0.0766849)^T$. The critical surfaces are rotationally symmetric. The motion field is similar to a magnetic field instead of being roughly parallel.

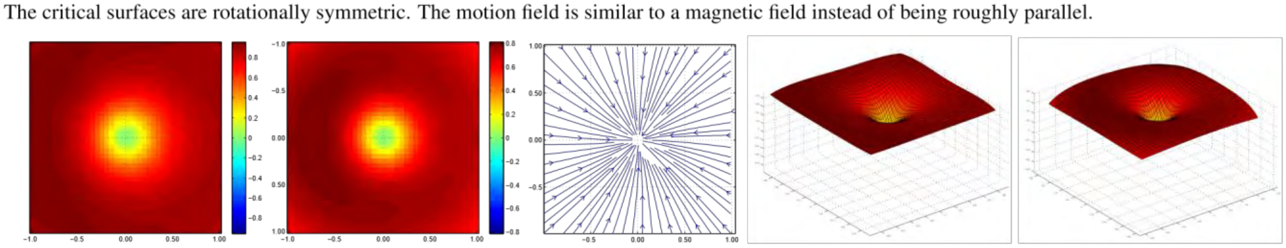

(c) $t_1 = t_2 = (-0.01, 0, -1)^T$, $\omega_1 = (0, 0.01, 0.05)^T$, $\omega_2 = (0, 0.099, 0.05)^T$. The translations are close to being forward in this example.

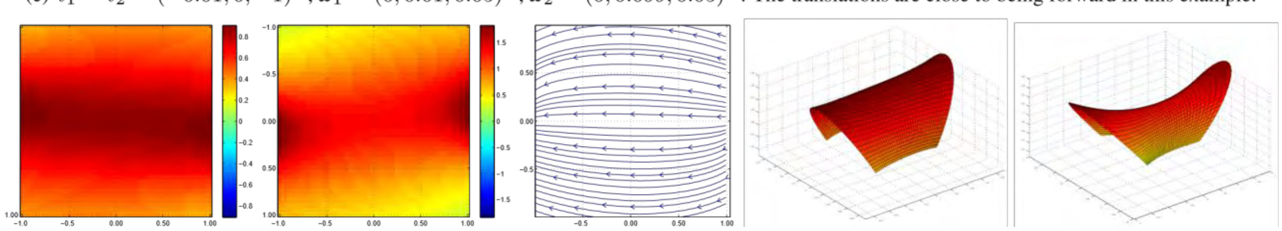

Z Z p^0 $Z\,p$ $Z\,Fp$

-0.5

0.00

0

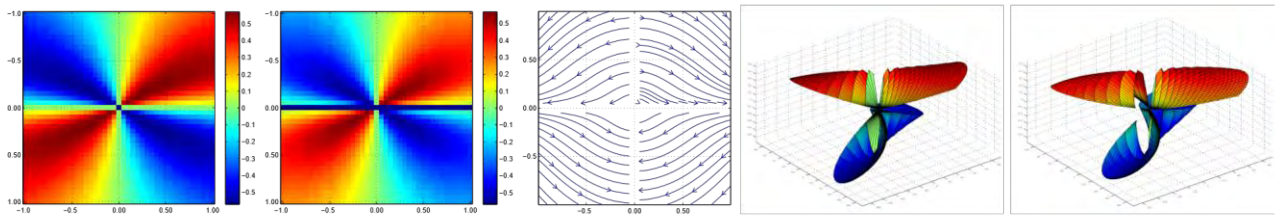

(e) $t_1 = t_2 = \omega_1 = \omega_2 = (1,0,0)^T$. Instead of being perpendicular, the translation and rotation are parallel in this example.

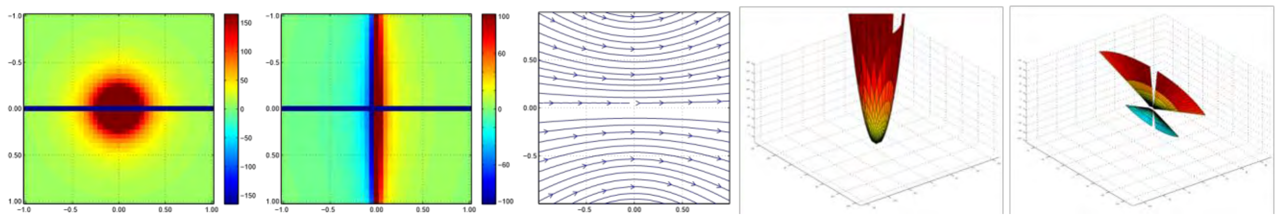

(d) $t1 = (0.850138,-0.526560,0)^T$, $t_2 = (0.992789,-0.119871,0)^T$, $\omega_1 = (0.600179,0.419835,0)^T$, $\omega_2 = (0.080059,0.179102,0)^T$.

(f) $t_1 = (1,0,0)^T$, $t2 = (0,0,1)^T$, $\omega_1 = \omega_2 = (0,1,0)^T$. The second camera has forward motion, and the first surface is rotationally symmetric.

Figure 2. Critical surface examples created with identity cameras and a radial distortion function: $f(r^2) = 1 + 0.1r^2 + 0.012r^4$. From left to right are 1) the first depthmap, 2) the second depthmap, 3) motion field direction, 4) first critical surface, 5) second critical surface. Note only the sub-portion of the critical surface corresponding to the $[-1,1] \times [-1,1]$ image region is visualized.

problem can be obtained by setting $f = 1$ and $f^0 = 0$, which become the well-known simpler ruled quadrics:

$$(P \times (\omega_2 - \omega_1)) \cdot (t_2 \times P) + (t_2 \times t_1)^T P = 0. \qquad (10)$$

For many camera configurations, the critical surface for radial distortion self-calibration is in fact similar to the corresponding ruled quadrics, and can be seen as a distorted version of the counterpart. An example configuration with such critical surfaces can be found in Figure 2(d).

When the camera motion is known to be pure translation $\omega_1 = \omega_2 = 0$ or pure rotation $t_1 = t_2 = 0$, critical surfaces do not exist in the distortion-free case. When radial distortion is considered, there exist the previously discussed critical motions but no additional critical surfaces. It is already shown that radial distortion is not ambiguous for pure rotation except for rotations around the optical axis. Similarly, radial distortion is found not ambiguous for pure translation except when it is along the optical axis.

The biggest difference regards the case of known rotation $\omega_1 = \omega_2 \neq 0$ and known translation $t_1 = t_2 \neq 0$ (ignoring scale). Under such conditions, it is known that critical surfaces do not exist for the distortion-free problem [5]. In contrast for radial distortion self-calibration, critical surfaces still exist, even when

both rotation and translation are known: $t_1 - t_2 = \omega_1 - \omega_2 = 0$. This can be seen from Equation 4 because $f^0 \neq 0$. See Figure 2 for examples of such critical surfaces.
The new kind of critical surfaces are particularly interesting. It shows that 3D reconstruction with unknown radial distortion may still be ambiguous even when translation and (or) rotation are correctly estimated.

1.2. Additional rotation around the optical axis

For any configuration of motion and surface that satisfies Equation 2, let us consider an additional rotation velocity around the optical axis such that $\omega_1^\delta = \omega_1 + \delta\hat{z}$ and $\omega_2^\delta = \omega_2 + \delta\hat{z}$. The addition to the left side of Equation 2 is $(Fp)\times(\delta\hat{z}) = f\delta(p\times\hat{z})$, and is equal to the addition to the right side $F(p \times (\delta\hat{z})) = f\delta(p \times \hat{z})$. Therefore, Equation 2 still holds for $\{t_1, \omega_1^\delta, t_2, \omega_2^\delta\}$ with the same Z_1 and Z_2.
That is, equal additions to the rotation velocities around the optical axis does not change the critical surfaces, despite the changes in the motion fields.

2. An interesting degenerate case

As shown by the polynomial terms of different degrees in Equation 3, critical surfaces are complicated in general. We are interested in possible common divisors for those terms, so that the depth in Equation 4 can be simplified.

2.1. A common polynomial divisor

An interesting configuration arises during our analysis. We find Equation 3 of the first critical surface has a second order polynomial factor as follows:

$$\Phi = p^T t_1 (t_2 \times \hat{z})^T p, \tag{11}$$

when the following conditions are met:

$$t_1\cdot\hat{z} = t_2\cdot\hat{z} = 0,\ t_1 \times t_2 = 0, \text{ and } t_1\cdot t_2 \neq 0;$$

$$(\omega_1 - \omega_2)\cdot\hat{z} = 0 \text{ and } t_1\cdot\omega_1 = t_2\cdot\omega_2 = 0. \tag{12}$$

The camera motions can be viewed as the differential mode of one of the following well known cases:

- Moving on a sphere while pointing to center [16]. Orbital motion with additional rotation around the optical axis.
- Moving on a plane that is perpendicular to the viewing direction. This can be seen as moving on an infinite sphere ($\omega \times \hat{z} = 0$) in the above case.

It can be seen that t_1, t_2, $(\omega_1\times\hat{z})$, and $(\omega_2\times\hat{z})$ are parallel. Note critical surfaces will not exist for the distortion-free problem due to the *known translation* $t_1 \times t_2 = 0$.
We first try to simplify the cross products that involve Fp, that is, $(Fp)\times\omega_2 - F(p\times\omega_1)$. Using the invariance discussed in Section 5.2, we can assume $\omega_1\cdot\hat{z} = \omega_2\cdot\hat{z} = 0$ from $(\omega_1 - \omega_2)\cdot\hat{z} = 0$ without changing the critical surfaces. By using the fact $p = (p - \hat{z}) + \hat{z}$, we find

$$\begin{aligned}
&(Fp) \times \omega_2 - F(p \times \omega_1)\\
&= f(p - \hat{z}) \times \omega_2 + \hat{z} \times \omega_2 - (p - \hat{z}) \times \omega_1 - f(\hat{z} \times \omega_1)\\
&= (p - \hat{z}) \times (f\omega_2 - \omega_1) + \hat{z} \times (\omega_2 - f\omega_1),
\end{aligned} \tag{13}$$

Under the proposed conditions, we can prove the terms in the numerator and the denominator of Equation 4 divisible by Φ. By removing the dot-products of the perpendicular terms that produce zeros and by expanding the quadruple product, we can transform as follows:

$$\begin{aligned}
&\big((Fp) \times \omega_2 - F(p \times \omega_1)\big) \cdot (t_2 \times Fp)\\
&= \begin{pmatrix} (p-\hat{z}) \times (f\omega_2 - \omega_1) \\ + \hat{z} \times (\omega_2 - f\omega_1) \end{pmatrix} \cdot \begin{pmatrix} f\,t_2 \times (p - \hat{z}) \\ + t_2 \times \hat{z} \end{pmatrix}\\
&= \Big((p - \hat{z}) \times (f\omega_2 - \omega_1)\Big) \cdot \Big(f\,t_2 \times (p - \hat{z})\Big)\\
&= \big((p - \hat{z}) \cdot t_2\big)\ \big((p - \hat{z}) \cdot (f^2\omega_2 - f\omega_1)\big)\\
&= -p^T\big((f^2\omega_2 - f\omega_1) \times \hat{z}\big)\,(t_2 \times \hat{z})^T p,
\end{aligned}$$

which can be divided by Φ because $t_1 \parallel (\omega_1\times\hat{z}) \parallel (\omega_2\times\hat{z})$. Similarly, the term $2f^0\,(p^Tp)p^T(\omega_1 \times \hat{z})(t_2 \times \hat{z})^Tp$ in the denominator can be divided by Φ because $t_1 \parallel (\omega_1\times\hat{z})$. As for the terms in the numerator, both $(t_1\cdot\hat{z})(p^Tp)(t_2\times\hat{z})^Tp$ and $(t_2 \times Ft_1)^T Fp$ become zero, and the only left term is $2f^0 p^T t_1(t_2 \times \hat{z})^T p = 2f^0\,\Phi$.

The common divisor Φ itself defines two critical planes $t_1^T p = 0$ and $(t_2 \times \hat{z})^T p = 0$. The two planes are not too interesting because the camera center is on the planes and they are also perpendicular to the image plane. We will leave the planes here and focus on the simplified depth.

2.2. Rotationally symmetric surfaces

By using the common divisor Φ, the first critical surface becomes much simplified

$$\begin{aligned}
Z_1 &= \frac{2f'\,p^T t_1 (t_2 \times \hat{z})^T p}{\begin{pmatrix} -p^T\big((f^2\omega_2 - f\omega_1) \times \hat{z}\big)\,(t_2 \times \hat{z})^T p \\ +2\,f'\,(p^Tp)\,p^T(\omega_1 \times \hat{z})\,(t_2 \times \hat{z})^T p \end{pmatrix}}\\
&= \frac{2\,(t_1 \cdot t_2) f'}{\begin{pmatrix} -(t_2 \cdot (\omega_2 \times \hat{z}))f^2 + (t_2 \cdot (\omega_1 \times \hat{z}))f \\ +2\,(t_2 \cdot (\omega_1 \times \hat{z}))(p^Tp)f' \end{pmatrix}},
\end{aligned} \tag{14}$$

which gives a single depth value for each image circle $r^2 = x^2 + y^2 = p^T p - 1$. The resulting critical surface is rotationally symmetric around the optical axis.

The second critical surface can be solved correspondingly using the relationship between the two depthmaps. Equation 13 allows the the following simplification:

$$((Fp) \times \omega_2 - F(p \times \omega_1)) \cdot (\hat{z} \times p) =$$

$$(\hat{z} \times (\omega_2 - f\,\omega_1)) \cdot (\hat{z} \times p).$$

Accordingly, the second critical surface is simplified to

$$\begin{aligned} Z_2 &= \frac{Z_1\, t_2 \cdot (\hat{z} \times p)}{(F t_1 - Z_1\, (\hat{z} \times (\omega_2 - f\,\omega_1))) \cdot (\hat{z} \times p)} \\ &= \frac{(t_1 \cdot t_2)\, Z_1}{(t_1 \cdot t_1)\, f - t_1 \cdot (\hat{z} \times (\omega_2 - f\,\omega_1))\, Z_1}, \end{aligned} \tag{15}$$

which is again rotationally symmetric.[1] Two examples of such critical surface are given in Figure 2(a) and 2(b). The pair of critical surfaces are both rotationally symmetric, but have different curvatures and even different curvature signs.

For a limited camera viewing angle, the portion of visible critical surfaces can be near-spherical, near-planar, or even a perfect plane depending on the motion and radial distortion function. For example, when $f(r^2) = 1/(1-\lambda r^2)$ and $\omega_1 \times \hat{z} = 0$, we are given a constant depth $Z_1 = \frac{4\lambda\,(t_1 \cdot t_2)}{t_2 \cdot (\hat{z} \times \omega_2)}$.

Let us revisit the UAV capture in Figure 1(a), where the camera moves parallel to the ground and the camera points to the ground. The visible surface relative to each camera is near-planar and thus have caused the ambiguity in radial distortion estimation.

2.3. Experiments

We devise two synthetic image sequences to verify the radial distortion ambiguity and demonstrate its impact on multi-view 3D reconstruction. We feed noise-free feature coordinates and perfect matches to VisualSFM [19], and compare the automatically reconstructed models to the ground-truth models. Although the reconstruction method is not velocity-based, we expect the same ambiguity with densely sampled image sequences.

[1] There exist other configurations where only one critical surface is rotationally symmetric. For example, when $t_1 \cdot \hat{z} = (\omega_1 - \omega_2) \cdot \hat{z} = t_1 \cdot \omega_1 = t_1 \cdot \omega_2 = 0$ and the second camera moves forward $t_2 \times \hat{z} = 0$, only the first critical surface is rotationally symmetric $Z_1 = \frac{t_1 \cdot t_1}{t_1 \cdot (\hat{z} \times (\omega_2 - f\,\omega_1))}$. See Figure 2(f) for an example.

First, as shown in Figure 3, we move a camera above a planar point grid at a constant height and keep the camera pointing to the plane. The distorted images are generated for the radial distortion $f(r^2) = 1 + \lambda r^2$, where $\lambda = 0.2$. This can be seen as an ideal version of the capture in Figure 1(a). Similar to the real capture, the automatic reconstruction of the synthetic dataset produces an incorrect distorted 3D model due to the ambiguity of radial distortion. Second, we use a point grid on a perfect sphere. The camera moves on a co-centered outer sphere and points to the sphere center. The distorted images are generated for the radial distortion $f(r^2) = 1+\lambda r^2$, where $\lambda = -0.2$. The spherical surface is rotationally symmetric and ambiguous for the reconstruction. As shown in Figure 4, the automatic reconstruction produces a concave surface instead.

The experiments show that multi-view reconstruction can fail to self-calibrate radial distortions under certain critical configurations. The distortion of the reconstruction is caused locally by the curvature difference between the critical surface pairs and globally by the curvature error accumulation from the persistent ambiguity in the entire capture.

Typical SfM systems initialize the radial distortions of new cameras to zero and rely on bundle adjustments to optimize the parameters. We observe a tendency to under-estimate the radial distortions in near-degenerate configurations, which can be partially explained by the zero initialization. The ambiguity of radial distortion is likely to cause significant inaccuracy when the radial distortions are sever or when the initial estimations are too inaccurate. Also note there would be more ambiguity when using more radial distortion parameters, for example, $f(r^2) = 1 + \lambda_1 r^2 + \lambda_2 r^4$ compared to $f(r^2) = 1 + \lambda_1 r^2$.

3. Conclusions and future work

This paper presents the critical configurations for radial distortion self-calibration under a general radial distortion model. It is shown that radial distortion introduces a new kind of ambiguity into SfM. Unlike the pure linear camera parametrization, critical surfaces exist even for known translations and known rotations due to radial distortion. In particular, this paper demonstrates the practically important critical configurations that should be avoided in real capture for radial distortion self-calibration.

This paper is not meant to be a complete study of all possible ambiguities related to radial distortion. The author wishes to conduct a numerical stability study on neardegenerate congurations and extend the investigation from continuous motion to discrete

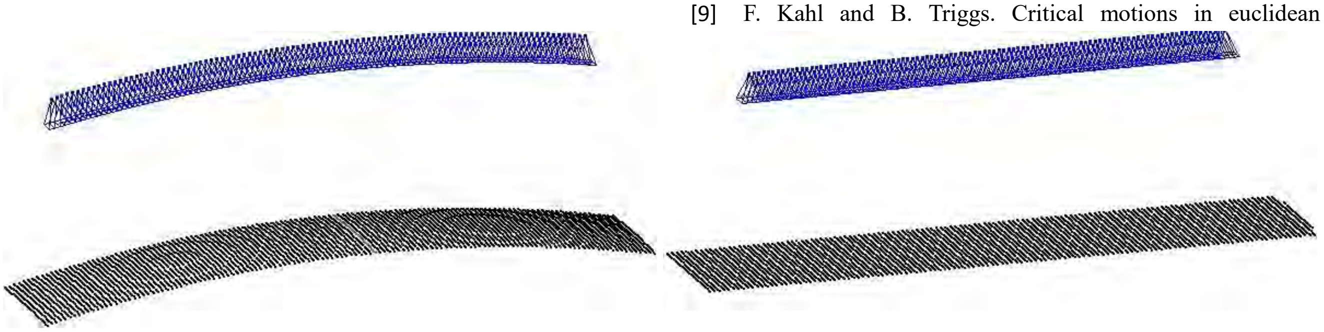

(a) The automatic reconstruction estimates an incorrect $\lambda^0 = 0.02$ (b) The ground-truth reconstruction using the known $\lambda = 0.2$

Figure 3. Reconstruction of a planar point grid. The blue pyramids are the cameras and the black dots are the reconstructed points.

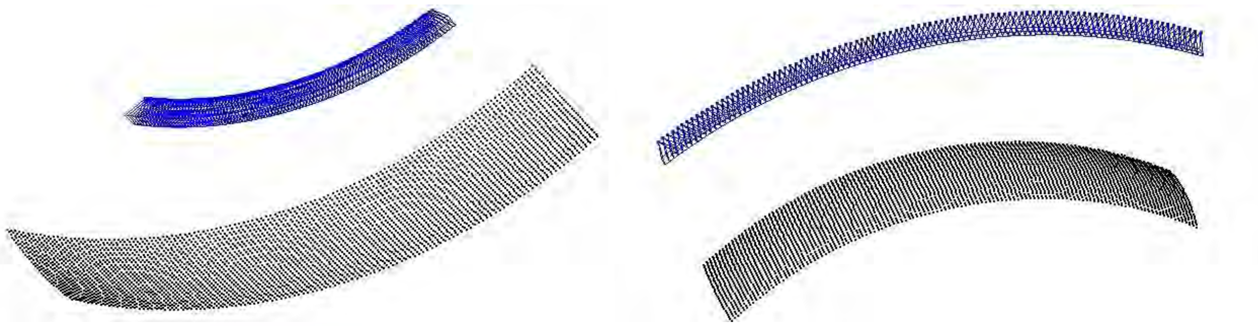

(a) The automatic reconstruction estimates an incorrect $\lambda^0 = 0.025$ (b) The ground-truth reconstruction using the known $\lambda = -0.2$ Figure 4. Reconstruction of a point grid on a sphere. The blue pyramids are the cameras and the black dots are the reconstructed points.

viewpoints in the future.

Acknowledgements The author sincerely thanks Thomas Groninger for providing the two UAV datasets.¨

References

[1] S. Agarwal, N. Snavely, I. Simon, S. M. Seitz, and R. Szeliski. Building Rome in a day. In *ICCV*, 2009.

[2] J. H. Brito, R. Angst, K. Koser, and M. Pollefeys. Radial¨ distortion self-calibration. In *CVPR*, 2013.

[3] D. Crandall, A. Owens, N. Snavely, and D. P. Huttenlocher. Discrete-continuous optimization for large-scale structure from motion. In *CVPR*, 2011.

[4] R. I. Hartley. Ambiguous configurations for 3-view projective reconstruction. In *ECCV*, pages 922–935, 2000.

[5] B. K. P. Horn. Motion fields are hardly ever ambiguous. *IJCV*, 1(3):259–274, 1987.

[6] F. Kahl. Critical motions and ambiguous euclidean reconstructions in auto-calibration. In *ICCV*, volume 1, pages 469–475, 1999.

[7] F. Kahl and R. Hartley. Critical curves and surfaces for euclidean reconstruction. In *ECCV*, pages 447–462, 2002.

[8] F. Kahl, R. Hartley, and K. Astrom. Critical configurations for n-view projective reconstruction. In *CVPR*, pages 158–163, 2001.

[9] F. Kahl and B. Triggs. Critical motions in euclidean structure from motion. In *CVPR*, volume 2, 1999.

[10] F. Kahl, B. Triggs, and K. Astr˚ om.¨ Critical motions for auto-calibration when some intrinsic parameters can vary. *JMIV*, 13(2):131–146, 2000.

[11] H. C. Longuet-Higgins. Visual ambiguity of a moving plane. *Proceedings of The Royal Society of London, Biological Sciences*, pages 165–175, 1984.

[12] S. Maybank. Theory of reconstruction from image motion. 1993.

[13] S. J. Maybank. The angular velocity associated with the optical flow field due to a single moving rigid plane. In *ECAI*, pages 641–644, 1984.

[14] B. Micuˇ sˇ´ık and T. Pajdla. Structure from motion with wide circular field of view cameras. *TPAMI*, 28(7):1135–1149, 2006.

[15] N. Snavely, S. Seitz, and R. Szeliski. Photo tourism: exploring photo collections in 3D. In *SIGGRAPH*, pages 835–846, 2006.

[16] P. Sturm. A case against kruppa's equations for camera self-calibration. *TPAMI*, 22(10):1199–1204, 2000.

[17] P. F. Sturm. Critical motion sequences for monocular self-calibration and uncalibrated euclidean reconstruction. In *CVPR*, pages 1100–1105, 1997.

[18] P. F. Sturm. Critical motion sequences for the self-calibration of cameras and stereo systems with variable focal length. In *BMVC*, 1999.

[19] C. Wu. VisualSFM: A visual structure from motion system,

2011. http://ccwu.me/vsfm.

[20] C. Wu. Towards linear-time incremental structure from motion. In *3DV*, 2013.

[21] C. Wu, S. Agarwal, B. Curless, and S. M. Seitz. Multicore bundle adjustment. In *CVPR*, 2011.